JOURNAL OF MATERIALS SCIENCE 26 (1991) 5433–5444

Monte-Carlo simulation of multiple fracture in the transverse ply of cross-ply graphite–epoxy laminates

SHOJIRO OCHIAI*, P. W. M. PETERS, K. SCHULTE
Deutsche Forschungsanstalt für Luft- und Raumfahrt, Institut für Werkstoff-Forschung, 5000 Köln 90, FRG

KOZO OSAMURA
Department of Metallurgy, Kyoto University, Sakyo-ku, Kyoto 606, Japan

Graphite–epoxy cross-ply laminates generally show multiple fracture of the transverse ply at higher applied stress. This phenomenon is described by means of a Monte Carlo simulation method based on the assumption that the strength of the transverse ply obeys a two-parameter Weibull distribution function. The main results show that the smaller the scatter of strength of the 90°-ply (i.e. the larger the shape parameter at a constant mean strength of the Weibull distribution), the higher becomes the threshold for the multiple fracture to occur, and the more rapidly the length of 90°-ply segments decreases with increasing applied stress once multiple fracture takes place. The methods to determine the shape and scale parameters of the Weibull distribution for the strength of the 90°-ply proposed by Manders *et al.* and Peters are proved to be useful even for a small number of test specimens. When the interfacial bond strength between 0°- and 90°-plies is low, saturation of 90°-ply cracking occurs at higher applied stress. The stress-carrying capacity and stiffness of the composites as a whole are reduced by multiple fracture of the 90°-ply. This reduction is more pronounced at increasing applied stress or at a larger number of transverse cracks, especially when the interfacial bond strength is low.

1. Introduction

In graphite–epoxy laminates with a 0/90/0 stacking sequence, the strain at which failure in the 90°-ply occurs is generally less than that of the 0°-ply. Therefore, a sample of these laminates under tension shows fracture of the transverse ply prior to 0°-ply failure. The breakdown of the 90°-ply causes a reduction of the bearing capacity of the composite and a redistribution of stresses in the 90°- and 0°-plies. However, as the 0°-ply has a higher load-bearing capacity than the 90°-ply, the loss of stress in the transverse ply as a result of cracking is completely compensated by the 0°-plies. This causes the transverse ply to fail repeatedly before the specimen finally fails [1]. This phenomenon, known as multiple fracture, has extensively been studied by many workers [2–13]. It has been observed not only in cross-plied polymer matrix composites, but also in unidirectional metal matrix composites [14–18].

In cross-plied polymer matrix composites the strain at the occurrence of the first crack in the transverse ply is higher when the thickness of the 90°-ply is less due to the constraining effect. This has been explained by Parvizi *et al.* [2] in terms of a fracture mechanics approach employing a finite element method. The crack spacing (length of segments of the transverse ply) decreases with increasing applied stress if the interface does not fail and if the matrix does not yield [2, 5, 7, 8, 11, 12]. The crack spacing is also affected by the effect of constraint. Thus, the 90°-ply in angle-(cross-) ply laminates behaves differently from the unidirectional laminate in transverse tension.

Although multiple fracture of the 90°-ply cannot be predicted beforehand, it has been demonstrated by the analysis of experimental data that the apparent strength can be described by the two-parameter Weibull distribution function [5, 7, 12]. Manders *et al.* [5] (the MCJR method) and Peters and co-worker [7, 12] (the P method) proposed simple methods to deduce the shape and scale parameters of Weibull distributions which describe the strength of the transverse ply.

In this work, multiple fracture of the 90°-ply in $0_2/90_4/0_2$, $0_2/90_6/0_2$ and $0_2/90_{12}/0_2$ graphite/epoxy laminates was simulated by means of the Monte Carlo method making use of several Weibull distributions. This Monte Carlo method has been employed previously to describe the multiple fracture phenomenon of a single fibre embedded in a metal matrix [16] and that of a coating film on a metal wire [17].

* *Present address*: Department of Metallurgy, Kyoto University, Sakyo-ku, Kyoto 606, Japan.

0022–2461/91 $03.00 + .12

The accuracy of the determined Weibull parameters by the MCJR and P methods was investigated. Further, the influence of interfacial debonding on multiple fracture was investigated and the reduction in stiffness of a composite due to multiple fracture was determined.

2. Experimental procedure

Graphite/epoxy laminates with a stacking sequence of $0_2/90_4/0_2$, $0_2/90_6/0_2$ and $0_2/90_{12}/0_2$ were produced from Fibredux 914C prepregs. The conditions of specimen preparation and testing were given previously [7, 12].

3. Computer simulation procedure

3.1. Calculation of stress distribution in a cracked 90°-ply

3.1.1. Model composite

The stress distribution in the 0^0- and 90°-plies with cracks in the 90°-ply were calculated by using a shear lag analysis. Fig. 1 shows a schematic presentation of a cracked specimen. The thickness of the 0°- and 90°-plies is given by a_1 and a_2, respectively, as shown in (a), and the Young's moduli of the 0°- and 90°-plies by E_1 and E_2, respectively. The parameter x is the distance from the crack in the 90°-ply.

Owing to the difference in coefficient of thermal expansion between the 0°- and 90°-plies, the residual strains, e_{r1} and e_{r2}, exist in the x direction of the 0°- and 90°-plies, respectively. The residual strains satisfy Equation 1

$$2a_1E_1e_{r1} + a_2E_2e_{r2} = 0 \quad (1)$$

The mechanical stress in the composite, σ_c, at a strain of e before fracture of the 90°-ply is given by

$$\sigma_c = e(2a_1E_1 + a_2E_2)/(2a_1 + a_2) \quad (2)$$

If the 90°-ply fractures at the composite stress, σ_c, the stress that was carried by the 90°-ply is transferred to the 0°-ply. Now the 0°-ply carries all applied load at $x = 0$. Noting the ultimate strength of the 0°- and 90°-plies as σ_{u1} and σ_{u2}, respectively, the condition for multiple fracture to occur, based on the model of Kelly and Tyson [1], is approximately given by

$$(\sigma_{u2}/E_2)(2a_1E_1 + a_2E_2) < (\sigma_{u1}/E_1)2a_1E_1 \quad (3)$$

3.1.2. Equations of stress equilibrium and boundary conditions

The stress distribution in the broken 90°-ply is affected by the interlaminar shear strength between 0°- and 90°-plies.

3.1.2.1. Strong interface. If the composite is stressed in tension and the 90°-ply remains intact, the strain of 0°- and 90°-plies are $e + e_{r1}$ and $e + e_{r2}$, respectively. If the 90°-ply fractures, additional displacements du_1 and du_2 arise in the 0°- and 90°-plies, respectively. In this case the stresses in the 0°- and 90°-plies, σ_1 and σ_2, respectively, are given by

$$\sigma_1 = (e + e_{r1} + du_1/dx)E_1 \quad (4)$$

$$\sigma_2 = (e + e_{r2} + du_2/dx)E_2 \quad (5)$$

The stress equilibrium equations can be expressed by

$$E_1a_1(d^2u_1/dx^2) = (G/b)(u_1 - u_2) \quad (6)$$

$$E_2a_2(d^2u_2/dx^2) = 2(G/b)(u_2 - u_1) \quad (7)$$

where G is the shear modulus and b the thickness of the shear transfer layer. Reifsnider *et al.* [10] have suggested $b = 0.0127$ mm and $G = 1.378$ GPa for graphite epoxy. Peters and Chou [12] suggested that the shear transfer layer is a resin-rich area of twice the fibre diameter ($b = 0.015$ mm) and that G is the shear modulus of the matrix, G_m (1.48 GPa). In the present work, the values suggested by Peters and Chou were used for the calculation.

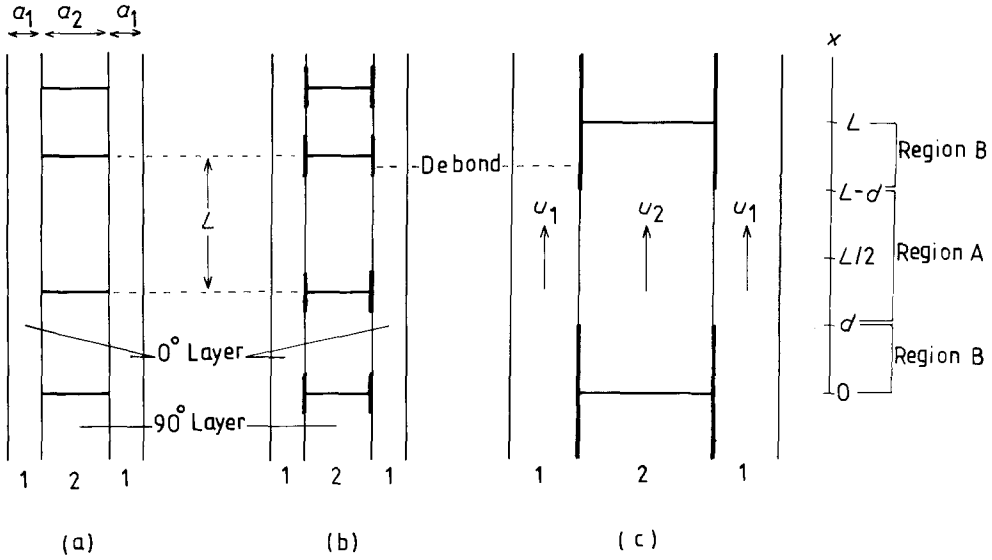

Figure 1 Schematic presentation of the model for the calculation of the stress distribution in the broken transverse ply for (a) a strong interfacial bond, and (b, c) for a weak bond.

For convenience, we set

$$E_2 a_2/(2E_1 a_1) = M \quad (8)$$

$$G_m/(E_1 a_1 b) = H \quad (9)$$

The general solutions of u_1 and u_2 are expressed as

$$u_1 = (A_1/k^2)\exp(-kx) + (A_2/k^2)\exp(kx) + A_3 x + A_4 \quad (10)$$

$$u_2 = (1/k^2 - 1/H)[A_1 \exp(-kx) + A_2 \exp(kx)] + A_3 + A_4 \quad (11)$$

where A_1 to A_4 are integral constants and k is given by

$$k = [H(1 + M)/M]^{1/2} \quad (12)$$

In order to estimate the values of A_1 to A_4, the following four boundary conditions are used.

(i) At $x = 0$, u_1 should be zero.

$$u_1(0) = 0 \quad (13)$$

(ii) At $x = 0$, the stress in the transverse ply is zero:

$$E_2\{e + e_{r2} + du_2(0)/dx\} = 0 \quad (14)$$

(iii) As the deformation behaviour of the segment of the 90°-ply with a length, L, is symmetric with respect to the middle at $x = L/2$, the additional displacements of the 0°- and 90°-plies are equal at $x = L/2$.

$$\Delta u_1(L/2) = \Delta u_2(L/2) \quad (15)$$

(iv) At any cross-section, the load is constant, being equal to $\sigma_c(2a_1 + a_2)$.

$$(2a_1 + a_2)\sigma_c = 2\sigma_1 a_1 + \sigma_2 a_2 \quad (16)$$

3.1.2.2. Weak interface. At $x = 0$, the highest shear stress is exerted in the shear zone between the 0°- and 90°-plies. If the shear strength, τ_i, is low, shear failure will occur when the exerted shear stress exceeds τ_i. This will take place at first at $x = 0$, and the debonded region will grow as schematically shown in Fig. 1b. In this paper, the region where no debonding occurs and the region where debonding occurs are named Regions A and B, respectively, as shown in Fig. 1c in which Region B covers $0 \leqslant x \leqslant d$ and $L - d \leqslant x \leqslant L$ and Region A $d \leqslant x \leqslant L - d$ where $2d$ is the length of the debonded region. As the stress distribution is symmetrical with respect to the middle between the cracks at $x = L/2$, the shear stress between the 0°- and 90°-plies at $x = L/2$ is always zero. Therefore, Region B cannot grow up to $x = L/2$: namely, in case of occurrence of interfacial failure, there always exists a Region A and a Region B. The equations of stress equilibrium for Region A are the same as those shown in Section 3.1.2.1, and u_1 and u_2 in this region are given by Equations 10 and 11, respectively.

Once interfacial failure has occurred (Region B), only frictional shear stress can exist in the shear zone. In this work, it is assumed that the frictional shear stress is low enough to be neglected. Under this assumption, the equations of stress equilibrium in Region B are given by

$$E_1 a_1(d^2u_1/dx^2) = 0 \quad (17)$$

$$E_2 a_2(d^2u_2/dx^2) = 0 \quad (18)$$

From Equations 17 and 18, we have

$$u_1 = B_1 x + B_2 \quad (19)$$

$$u_2 = B_3 x + B_4 \quad (20)$$

where B_1 to B_4 are integral constants.

In the case of the occurrence of shear zone failure, the unknown values are A_1 to A_4, B_1 to B_4 and d. These unknowns are determined with the aid of the following boundary conditions. In the following expressions, superscripts A and B refer to Regions A and B, respectively.

(i) At $x = 0$, u_1 should be zero.

$$u_1^B(0) = 0 \quad (21)$$

(ii) At $x = 0$, the stress in the 90°-ply is zero.

$$du_2^B(0)/dx = 0 \quad (22)$$

(iii) to (vi) At $x = d$, the displacement and stress should be continuous.

$$u_1^A(d) = u_1^B(d) \quad (23)$$

$$u_2^A(d) = u_2^B(d) \quad (24)$$

$$E_1[e + e_{r1} + du_1^A(d)/dx] = E_1[e + e_{r1} + du_1^B(d)/dx] \quad (25)$$

$$E_2[e + e_{r2} + du_2^A(d)/dx] = E_2[e + e_{r2} + du_2^B(d)/dx] \quad (26)$$

(vii) At $x = d$, the shear stress in the shear zone in Region A is equal to τ_i.

$$(G_m/b)[u_2^A(d) - u_1^A(d)] = \tau_i \quad (27)$$

(viii) At any cross-section, the load is constant, being equal to $\sigma_c(2a_1 + a_2)$.

$$\sigma_c(2a_1 + a_2) = 2a_1 E_1[e + e_{r1} + du_1^A(x)/dx] + a_2 E_2[e + e_{r2} + du_2^A(x)/dx] \quad (28)$$

(ix) As the deformation behaviour of the 90°-ply segment is symmetrical with respect to $x = L/2$, the displacements of the 0°- and 90°-plies are equal to each other at $x = L/2$.

$$u_1^A(L/2) = u_2^A(L/2) \quad (29)$$

3.2. Procedure of Monte Carlo simulation

The procedure of the Monte Carlo simulation for multiple fracture was nearly the same as that employed previously [16, 17]. In this paper, the procedure is briefly summarized.

1. The 90°-ply with an initial length, L_0, was divided into n elements with a length L_e as shown in Fig. 2a where the centre of the first and the last element are located at either end of the 90°-ply. The value of n was therefore equal to $L_0/L_e + 1$. In this work, L_e was taken to be 0.25 mm.

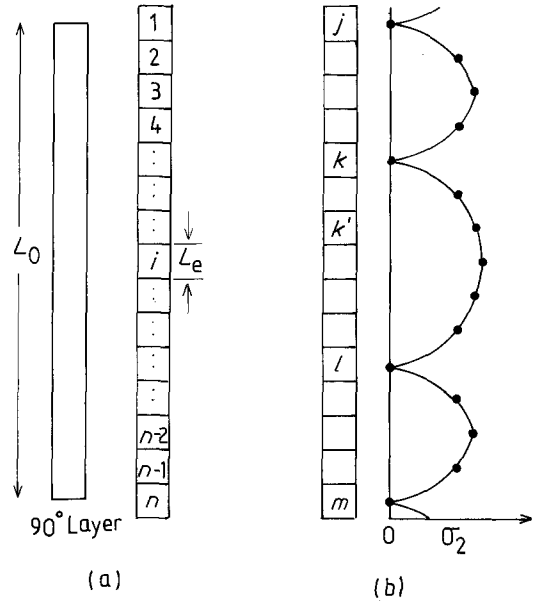

Figure 2 The transverse ply is divided into elements with a length of L_e. (a) A schematic illustration of the definition of the elements, and (b) the exerted tensile stress on each element, where the j, k, l and mth elements are broken already.

2. The strength distribution of the 90°-ply was given by the two parameter Weibull distribution [19], according to which the probability of failure, F, at a stress, σ, is expressed as

$$F = 1 - \exp[-l(\sigma/\sigma_0)^w] \quad (30)$$

where w and σ_0 are shape and scale parameters and l is the length.

3. The strength of elements was given by the Monte Carlo method: namely, a random value between 0 and 1.0 was generated for each element in the computer, and the strength of each element $S(i)$ was calculated from Equation 30 by substituting the random value as F.

4. The stress distribution in 90°-ply was calculated by the method shown in Section 3.1. The stress exerted at the mid-point of each element was taken as the exerted stress on the complete element, as shown in Fig. 2b. When the stress $\sigma_2(i)$ on the ith element exceeds the given strength $S(i)$, the element was judged to be fractured and the strength of this element was set at 0. For instance, when the j, k, l and mth elements are broken (namely when $S(j) = S(k) = S(l) = S(m) = 0$), and the exerted stress on the k' element is higher than the $S(k')$, the k' element breaks and the $S(k')$ is set at 0 at this stress level.

5. The strain of the composite as a whole was calculated as follows. If the 90°-ply is broken into p segments and the length of the qth segment is L_q, the displacement of the qth element at $x = L$ relative to $x = 0$ is given by $eL_q + 2\Delta u_2(L_q/2)$ where $\Delta u_2(L_q/2)$ is the displacement of the 90°-ply at the centre of the qth segments. Therefore the total displacement of the specimen from one end to the other is given by

$$\sum_{q=1}^{p} \{eL_q + 2\Delta u_2(L_q/2)\} \quad (31)$$

As the initial length of the composite was L_0, the strain e_c of the composite is given by

$$e_c = e + 2\left[\sum_{q=1}^{p} \Delta u_2(L_q/2)/L_0\right] \quad (32)$$

6. The stress level was raised in steps of 0.1 MPa from zero to the fracture stress of the specimen roughly given by

$$\sigma_{cu} = \sigma_{1u} V_1 \quad (33)$$

where σ_{1u} is the ultimate tensile strength of the 0°-plies and V_1 is the volume fraction of the 0°-plies.

The simulation experiment was mainly carried out for the $0_2/90_6/0_2$ laminate.

The average strength for 1 mm long segments of the 90°-ply, $\bar{\sigma}_2$, was taken to be 125 MPa and the values of w were determined based on the Weibull distribution: $\sigma_0 = 136$, 131 and 123 MPa for $w = 5$, 10 and 20, respectively. The values of the parameters used in the present simulation for $0_2/90_6/0_2$ were as follows: $a_1 = 0.25$ mm, $a_2 = 0.75$ mm, $E_1 = 128$ GPa, $E_2 = 9.5$ GPa, $G_m = 1.48$ GPa, $b = 0.015$ mm, $e_{r2} = 0.004$, $L_0 = 100$ mm, $L_e = 0.25$ mm and $\tau_i = 200$–500 MPa.

4. Results and discussion

4.1. Stress distribution in the 90°-ply

Fig. 3 shows the tensile stress distribution in the 90°-ply in the $0_2/90_6/0_2$ laminate for $L = 0.5$–5.0 mm at the composite stress $\sigma_c = 100$, 300 and 500 MPa for (a) a strong bond ($\tau_i = 400$ MPa in this case) and (b) a weak bond ($\tau_i = 250$ MPa).

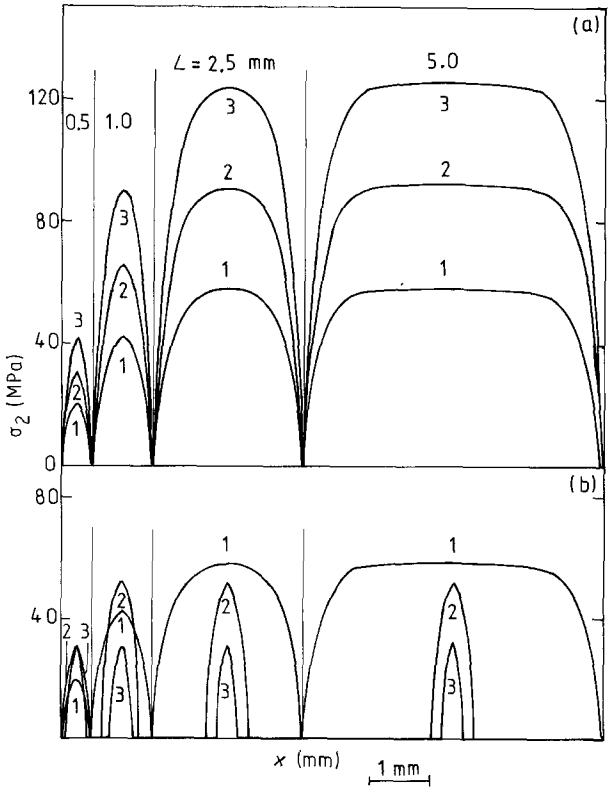

Figure 3 Stress distributions in the 90°-ply with $L = 0.5$–5.0 mm in the $0_2/90_6/0_2$ laminate at $\sigma_0 = (1)$ 100, (2) 300, (3) 500 MPa for (a) a strong, and (b) a weak interfacial bond. (a) No debonding, $\tau_i = 400$ MPa; (b) debonding, $\tau_i = 250$ MPa.

In case of a strong bond, σ_2 increases with increasing σ_c at any x except at $x = 0$ for any values of L. It is evident that the higher tensile stress is exerted on the longer 90°-ply segments. The maximum stress of the segments, $\sigma_{2,max}$ is found at $x = L/2$. Fig. 4a shows the variations of $\sigma_{2,max}$ for a high interlaminar shear strength for $L = 0.5$ to 5.0 mm as a function of σ_c. The $\sigma_{2,max}$ increases with increasing σ_c for any values of L but the $\sigma_{2,max}$ decreases with decreasing L at a given value of σ_c, as long as the segment length is shorter than double the ineffective length. This means that the long segments can be broken into shorter segments, because the longer the segments, the higher becomes the exerted tensile stress and therefore the higher the probability that the exerted stress reaches the tensile strength of the segments.

On the other hand, if the bond strength is low, debonding occurs in the shear zone and the efficiency of stress transfer to the 90°-segment becomes low, as known from Fig. 3b. The $\sigma_{2,max}$ increases with increasing σ_c within the range where no debonding occurs but it decreases after debonding as shown in Fig. 4b, where the arrows show the stresses at which interfacial debonding occurs. For instance, the $\sigma_{2,max}$ for the segment length $L = 5.0$ mm increases with increasing σ_c along AB where no debonding occurs, but it decreases along BC after debonding at B. It is interesting that the stress in the composite at debonding is dependent on the segment length: the shorter the length, the higher becomes the critical stress for the debonding to occur. As a result, the stress, $\sigma_{2,max}$, for $L = 0.5$ mm varies along DEC where debonding occurs at E.

$\sigma_{2,max}$ is essentially dependent on the interlaminar shear strength, τ_i, as shown in Fig. 5. The lower τ_i, the lower becomes the stress for debonding to occur. For instance, for $\tau_i = 200$ MPa, $\sigma_{2,max}$ varies along ABC, but for $\tau_i = 350$ MPa, it varies along AHI. In this way, the weak shear zone results in a low efficiency of stress transfer to the 90°-ply segments, leading to no further fracture of the segments. Therefore, with a weak shear zone it is expected that the number of cracks in the 90°-ply will show saturation, which will be ascertained by the present computer simulation.

The growth of debonded region (Region B) is very rapid just after the beginning of debonding, but it becomes relatively slow with increasing applied stress, σ_c, and finally the length of the debonded region, d, approaches $L/2$, as shown in Fig. 6.

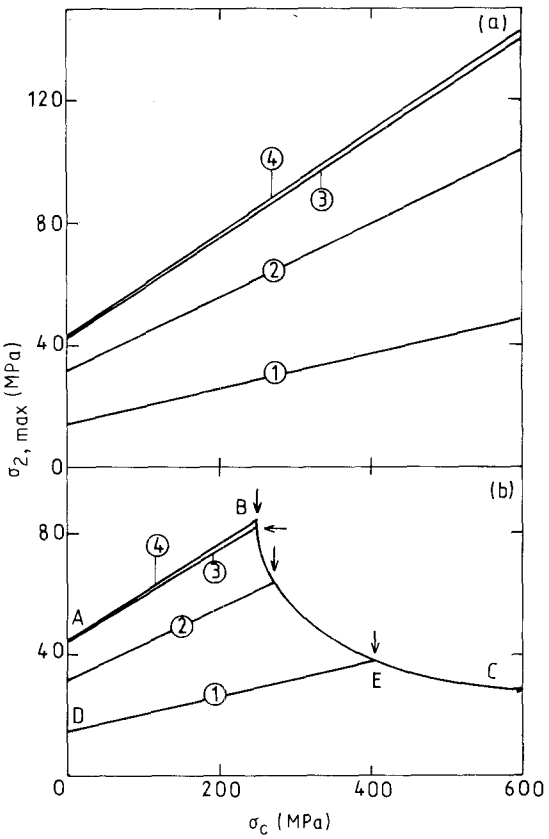

Figure 4 Variations of $\sigma_{2,max}$ as a function of σ_c for $L =$ (1) 0.5, (2) 1.0, (3) 2.5, (4) 5.0 mm in the $0_2/90_6/0_2$ laminate for (a) a strong, and (b) a weak interfacial bond. The arrows in (b) show the stresses at which debonding initiates. (a) No debonding, high τ_i; (b) debonding, $\tau_i = 250$ MPa.

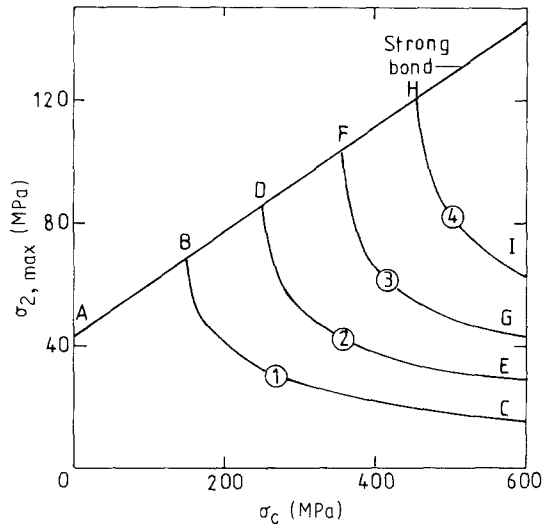

Figure 5 Influence of the interfacial bond strength, τ_i, on the variation of $\sigma_{2,max}$ for a given value of the segment length $L = 5$ mm in a $0_2/90_6/0_2$ laminate. $\tau_i =$ (1) 200, (2) 250, (3) 300, (4) 350 MPa.

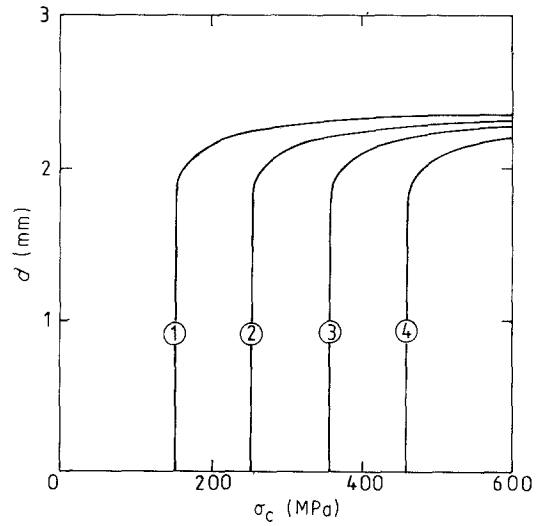

Figure 6 Growth of length of the debonded region, d, as a function of σ_c for $\tau_i =$ (1) 200, (2) 250, (3) 300, (4) 350 MPa for a given segment length of $L = 5$ mm. The variations of $\sigma_{2,max}$ in these cases are shown in Fig. 5.

4.2. Distribution of the length of segments of the 90°-ply

Fig. 7 shows an example of the results of the present computer simulation for the process of multiple fracture of the transverse ply in the $0_2/90_6/0_2$ laminate with a high interlaminar shear strength. The solid lines show the location of cracks in the 90°-ply. The 90°-ply is broken into more and more segments with increasing applied stress on the composite. The long segments tend to be broken into shorter ones with increasing applied stress, but fracture does not necessarily occur in the middle. Therefore the length of the segments is widely scattered in this example for $w = 5$. Fig. 8 shows an example of the distribution of lengths of segments for three different stress levels. At a low stress such as 350 MPa, the segment length varies strongly, but at a high stress such as 600 MPa, the lengths of the segments are within a relatively narrow range.

The scatter in the length of segments depends on the value of w. The smaller the value of w, the larger is the scatter, as typically shown in Fig. 9 where the average length of segments, $\bar{L}$, is nearly the same for both values of $w = 5$ and 20. This result can be explained by the fact that, when the scatter of strength of a 90°-ply is small, namely when the strength of each element shown in Fig. 2 is not very different from each other, the middle of the segments, on which the highest stress is exerted, tends to be broken.

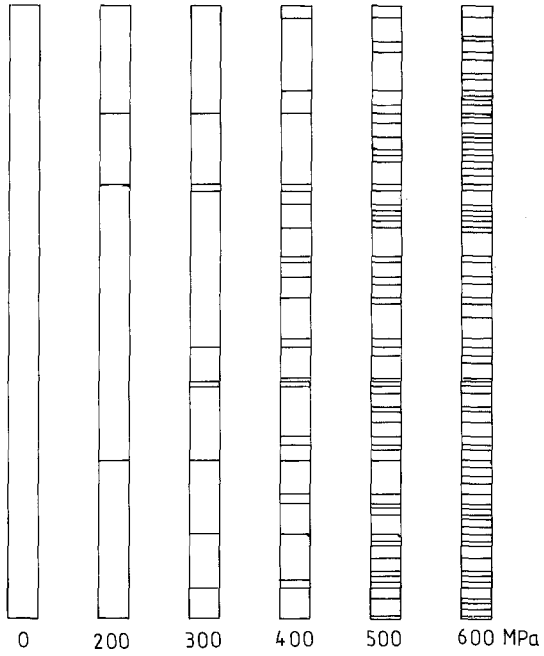

Figure 7 An example of multiple fracture in the 90°-ply of the $0_2/90_6/0_2$ laminate at various stress levels, obtained by the computer simulation for the Weibull distribution with $w = 5$ and $\sigma_0 = 136$ MPa.

high applied stress and further cracking will occur rather rapidly due to a small difference in strength of the elements.

4.3. Influence of scatter of the strength of the 90°-ply on multiple fracture

Fig. 10 shows some examples of the number of fractures, N_f, of the 90°-ply as a function σ_c. If the strength of the transverse ply has a large scatter ($w = 5$), first cracking occurs at a low applied stress and further cracking occurs rather gradually due to the large difference in strength of the elements. On the other hand, if the strength of the 90°-ply shows small scatter (large w), first cracking will occur at a relatively

4.4. Evaluation of the Weibull parameters from experimental data

As the fracture behaviour of a transverse ply in laminates is affected by the constraining effect as stated before, the fracture behaviour cannot be predicted from the transverse test of the unidirectional laminate only. Manders *et al.* [5] (the MCJR method) and Peters and co-worker [7, 12] (the P method) presented simple models to evaluate Weibull parameters of a 90°-ply in laminates from experimental results. These

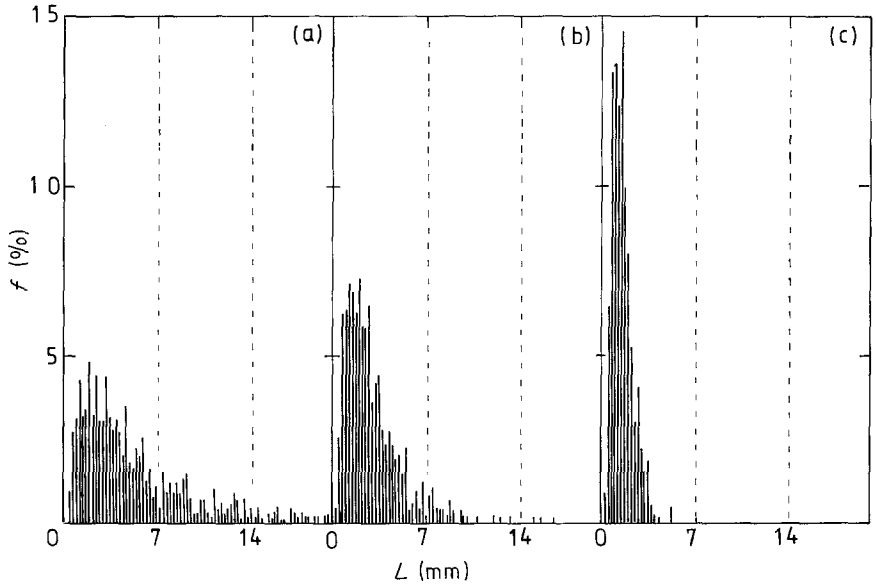

Figure 8 Distribution of the length of segments of the 90°-ply in a $0_2/90_6/0_2$ laminate at (a) $\sigma_c = 350$, (b) 450 and (c) 600 MPa. $w = 5$, $\sigma_0 = 136$ MPa.

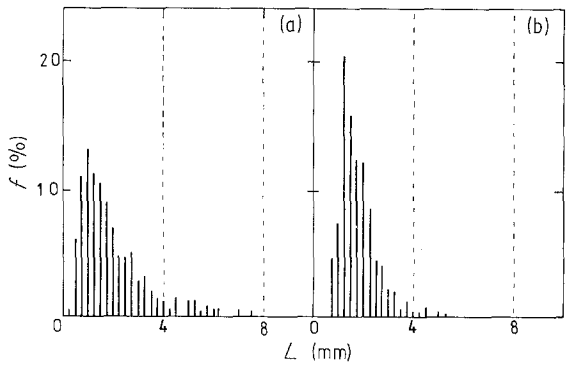

Figure 9 Comparison of the distribution of the length of segments of the 90°-ply in the $0_2/90_6/0_2$ laminate, (a) for $w = 5$, $\bar{L} = 2.0$ mm, with that of (b) for $w = 20$, $\bar{L} = 1.9$ mm, at $\sigma_c = 550$ MPa.

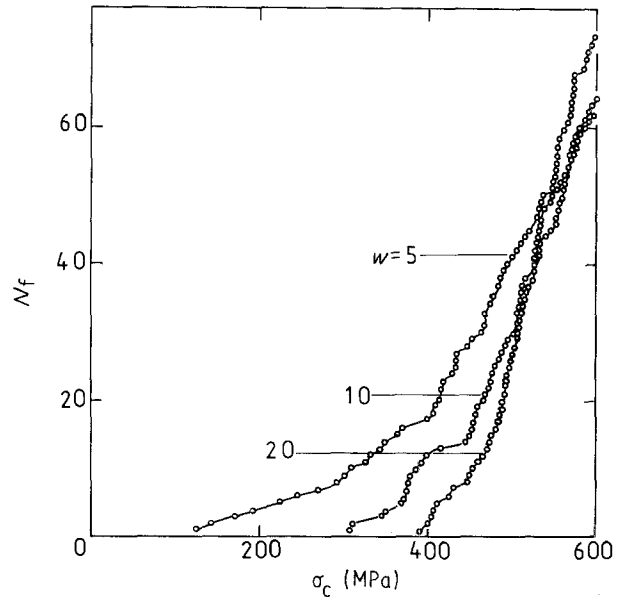

Figure 10 Influence of the scatter of strength of the transversy ply in the $0_2/90_6/0_2$ laminate on the number of cracks, N_f.

two methods are convenient for practical aim. However, generally, the experimental data show large scatter, which makes it difficult to determine the Weibull parameters from a small number of tests. On this point, the validity of these methods have not been checked until now. In this work, fracture data are generated by the simulation experiment, making use of a certain Weibull distribution, and from these generated data the Weibull parameters applying the MCJR- and P-methods are determined. The thus determined Weibull parameters are compared with the original parameters.

4.4.1. MCJR model [5]

The cracks appear at the weakest cross-section of the 90°-ply with a certain distribution along the length which depends on the applied strain. If it is assumed that the strengths of successive sections are independent and identically distributed, this will be a Poisson process. Applying the concept of risk of rupture, the cumulative distribution function of strength, S, for a length, L, under a given cross-sectional area of the 90°-ply is given by

$$S = 1 - \exp[-\Phi(\sigma)dx] \tag{34}$$

where $\Phi(\sigma)$ is the risk of rupture per unit length. When the cracks are widely spread, the integral in Equation 34 may be approximated, as below, by assuming a constant level of stress between cracks. Taking logarithmus gives

$$\ln(1 - S) = -\mu L \tag{35}$$

where μ is given by

$$\mu = \Phi(\sigma) = (\sigma_2/\sigma_0)^w \tag{36}$$

assuming a two-parameter Weibull distribution. Taking logarithms of Equation 36 leads to

$$\ln(\mu) = w\ln(\sigma_2) - w\ln(\sigma_0) \tag{37}$$

The values of μ and σ_2 can be determined experimentally. From the plot $\ln(\mu)$ versus $\ln(\sigma_2)$, w and σ_0 can be estimated.

The generated fracture data, which show large scatter in each specimen (run), are collected after the number of segments exceeded 500 at each stress level. Then, the MCJR method was evaluated first by these collected data. Figs 11 and 12 show the plots of $-\ln(1 - S)$ versus L for $w = 5$ and 20, respectively. If the fracture process is described by Equation 35, the graph of $-\ln(1 - S)$ against L should be linear with a slope μ and should pass through the origin. However, the curves in Figs 11 and 12 are not perfectly linear, nor do they pass through the origin. They are more linear at larger crack spacing, L. When straight lines are fitted to the linear portions of these curves, the intercept represents the distance at either side of a crack in which the probability of another crack to form is effectively zero. The MCJR model uses the straight portion for the evaluation of w and σ_0. From the slope μ in Figs 11 and 12 and the stress $\sigma_2 (= E_2(e + e_{r2}))$ at each stress level, σ_0 can be obtained, from Fig. 13 where $\ln(\mu)$ is plotted against $\ln(\sigma_2)$. The slope corresponds to w and the value of $\ln(\sigma_2)$ at $\ln(\mu) = 0$ corresponds to $\ln(\sigma_0)$. The values $w = 5.1$ and $\sigma_0 = 132.0$ MPa were determined from

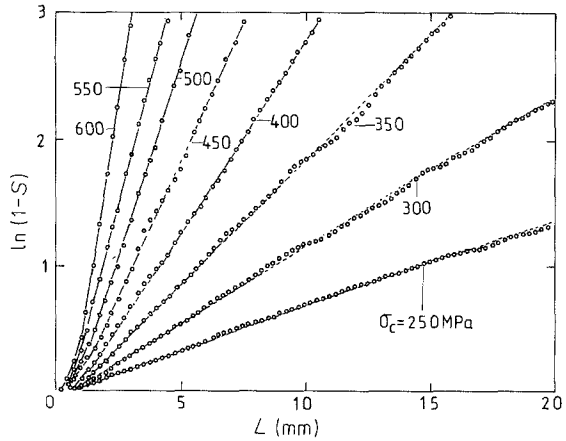

Figure 11 $-\ln(1 - S)$ plotted against L for the collected data for $w = 5$ and $\sigma_0 = 136$ MPa at various applied stresses (laminate $0_2/90_6/0_2$).

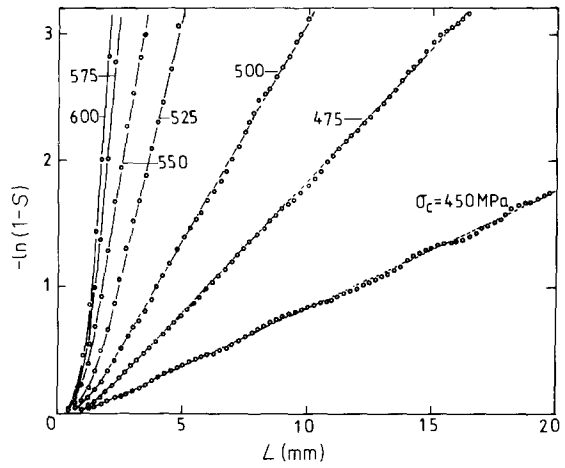

Figure 12 $-\ln(1-S)$ plotted against L for the collected data for $w = 20$ and $\sigma_0 = 128$ MPa at various applied stresses (laminate $0_2/90_6/0_2$).

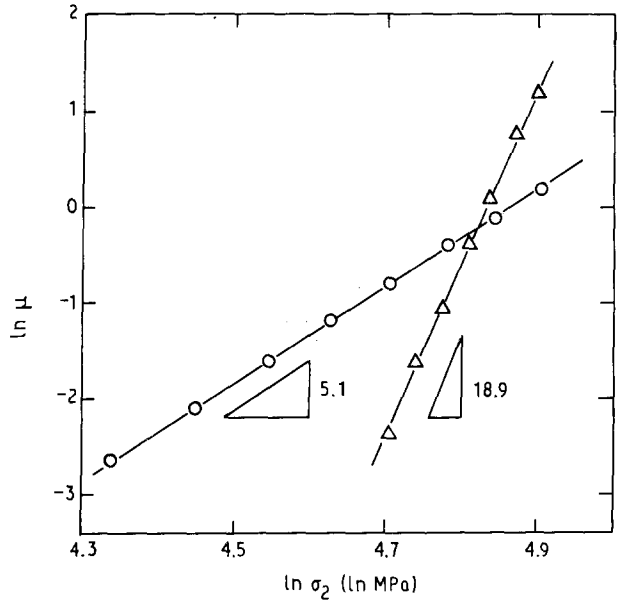

Figure 13 $\ln(\mu)$ plotted against $\ln(\sigma_2)$ for the $0_2/90_6/0_2$ laminate with $w = 5$ ($\sigma_0 = 136$ MPa) and $w = 20$ ($\sigma_0 = 128$ MPa) based on the MCJR [5] method for the simulated data.

Fig. 13, as shown in Table I. Comparing these values with $w = 5$ and $\sigma_0 = 136$ MPa which are the original Weibull parameters for the simulation experiment, the agreement is quite good. Also, for Weibull parameters $w = 20$ and $\sigma_0 = 129$ MPa, the values of w and σ_0 were determined to be 18.9 and 127 MPa, respectively, showing good agreement.

The results shown above indicate that the MCJR method is a good method to determine the Weibull parameters, if a sufficient number of segments can be obtained experimentally. However, in general, the number of test specimens is not large. For such a case, the experimental results will show scatter, which may lead to inaccuracies. This point will be discussed below.

Fig. 14 shows an example of the graph with $-\ln(1-S)$ as a function of the segment length L for one specimen (one run). The linearity is not good at each stress level. Furthermore, the data $-\ln(1-S)$ against L is different from specimen to specimen, as

TABLE I Comparison of the values of the Weibull parameters w and σ_0 determined from the generated data of the simulation experiment (Fig. 13) applying the MCJR method [5] with the original input parameters of the simulation experiment ($0_2/90_6/0_2$ laminate)

w		w	σ_0 (MPa)
5	Input	5.00	136
	Calculated	5.10	132
20	Input	20.0	128
	Calculated	18.9	127

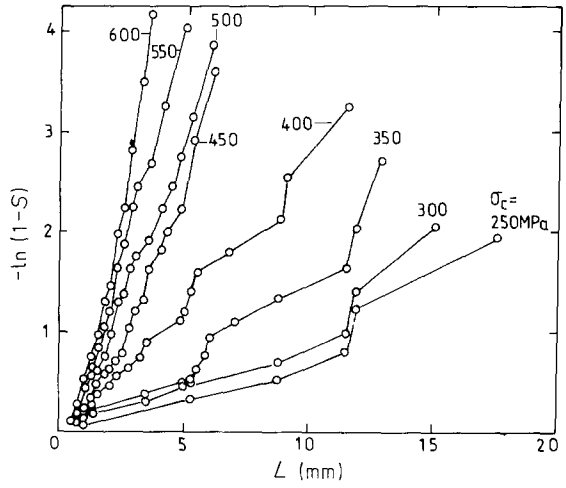

Figure 14 An example of $-\ln(1-S)$ plotted against L for one specimen (run) of the $0_2/90_6/0_2$ laminate with $w = 5$ and $\sigma_0 = 136$ MPa.

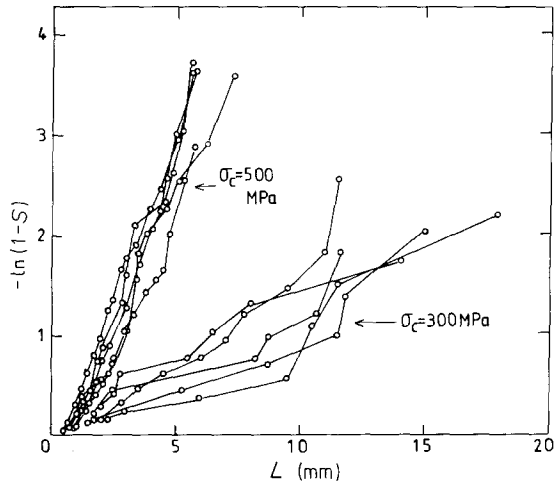

Figure 15 $-\ln(1-S)$ plotted against L at $\sigma_c = 300$ and 500 MPa for five $0_2/90_6/0_2$ specimens (runs) with $w = 5$ and $\sigma_0 = 136$ MPa showing a large scatter from specimen to specimen.

typically shown in Fig. 15 where the results for five specimens are plotted. Although, strict linearity is not found in Fig. 14, the data for each specimen approach a linear relationship in a first approximation. The straight lines in Fig. 14 are fitted by the least square method for $L > 1.5$ mm in order to obtain the values of μ, because the relation of $-\ln(1-S)$ to L is not linear in the range for $L < 1.5$ mm in Figs 11 and 12. The obtained values of μ are plotted against σ_2 on a

ln–ln scale, as shown in Fig. 16, where the results of five specimens for $w = 5$ and 20 are presented.

Although $\ln(\mu)$ is not necessarily a linear function of $\ln(\sigma_2)$ in the respective specimens, w and σ_0 are determined again by using the least square method. The result is shown in Table II. It is surprising that the determined values of w and σ_0 for each specimen are not so much different from the original Weibull parameters of $w = 5$ and $\sigma_0 = 136$ MPa and $w = 20$ and $\sigma_0 = 128$ MPa. If the results for the five specimens are averaged, the average values of w and σ_0 agree well with the original input values. These results indicate that with the MCJR method the Weibull parameters can be obtained with fairly high accuracy even if the number of specimens is small.

4.4.2. The P method [7, 12]

According to the calculation shown in Section 4.1, the stress in the 90°-ply is low close to existing cracks, so that new crack formation close to existing cracks is suppressed. This results in a certain crack spacing which is influenced, for example, by the strength distribution of the 90°-ply and the non-homogeneous stress distribution around cracks. Peters and co-worker [7, 12] considered that the 90°-ply consists of a chain of elements with a critical length, l_c, which is chosen such that the elements probably break only once. They chose somewhat arbitrarily the element length, l_c, to be twice the length in which 90% of the undisturbed stress is introduced in the 90°-ply. In case of the $0_2/90_6/0_2$ laminate, the element length, l_c, measures 0.83 mm [7].

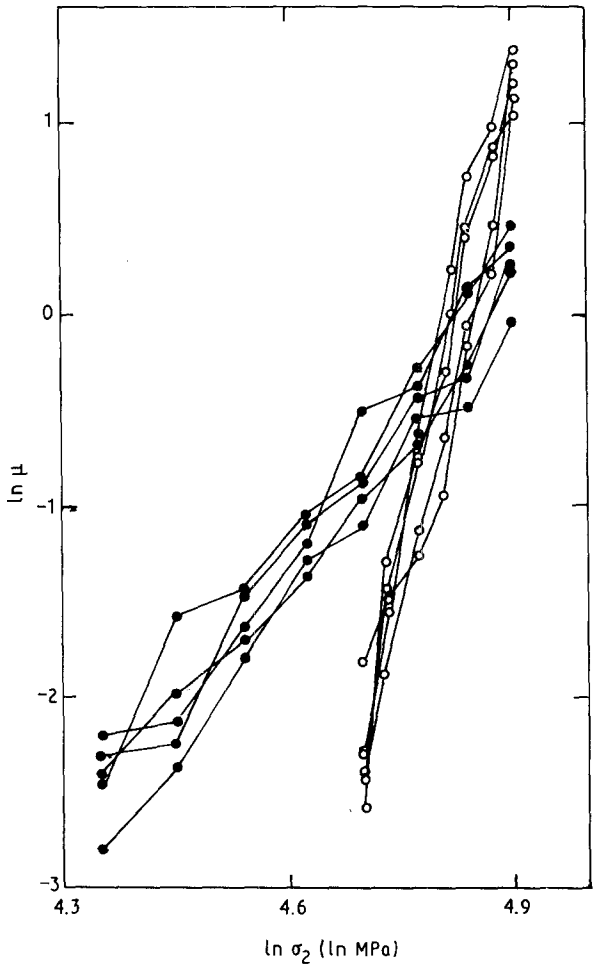

Figure 16 $\ln(\mu)$ plotted against $\ln(\sigma_2)$ for five $0_2/90_6/0_2$ specimens for (●) $w = 5$ ($\sigma_0 = 136$ MPa), together with those for (○) $w = 20$ ($\sigma_0 = 128$ MPa).

TABLE II The values of the Weibull parameters w and σ_0 for five specimens indicated in Fig. 16 calculated with the MCJR method [5] in comparison with the original input parameters of the simulation experiment for the $0_2/90_6/0_2$ laminate

w		w	σ_0 (MPa)
5	Calculated for each specimen	5.03	127
		4.68	133
		4.89	126
		4.58	135
		4.99	137
	Average	4.83	132
	Original input	5.00	136
20	Calculated for each specimen	18.2	126
		17.7	124
		17.6	125
		15.4	126
		22.5	124
	Average	18.2	125
	Original input	20.0	128

According to the P method, the stress in the 90°-ply is approximated to be zero for $|x| < l_c/2$ and to be equal to the undisturbed stress ($= E_2(e + e_{r2})$) for $|x| > l_c/2$. This simplification can lead to inaccuracy. At low loads with only a small number of element failures, the inaccuracy of the model is negligible. At high loads, more and more elements show an inhomogeneous stress distribution because of broken neighbours. Furthermore, a broken element can break again at high applied stress. Thus this model should be applied to the results at lower stress levels (see Fig. 17).

Equation 30 for $l = l_c$ and $\sigma = \sigma_2$ can be written as

$$\ln\ln(1 - F)^{-1} = w\ln(\sigma_2) - w\ln(l_c^{1/w}/\sigma_0) \quad (38)$$

The probability of failure, F, is calculated making use of

$$F = j/(N + 1) \quad (39)$$

where j represents the fracture order number and N the number of elements ($= L_0/l_c$). Substituting experimental values of F and σ_2 ($= E_2(e + e_{r2})$) into Equation 38, and plotting $\ln\ln(1 - F)^{-1}$ against $\ln(\sigma_2)$, one can determine the values of w and $\sigma_0/(l_c^{1/w})$ from the slope and the values of σ_2 at $\ln\ln(1 - F)^{-1} = 0$.

Fig. 17 shows the plots of $\ln\ln(1 - F)^{-1}$ against $\ln(\sigma_2)$. The data points in this figure are given by the average of 30 specimens (30 runs). The value of $\ln\ln(1 - F)^{-1}$ increases linearly with increasing value of $\ln(\sigma_c)$ in the range $\ln\ln(1 - F)^{-1} < -1.25$, but above this value it deviates from linearity due to the reason stated already. The linearity between $\ln\ln(1 - F)^{-1}$ and $\ln(\sigma_2)$ for relatively low values of F makes it possible to determine the values of Weibull parameters. The thus calculated values of w and σ_c are summarized in Table III. Good agreement between the original input and the determined values suggests

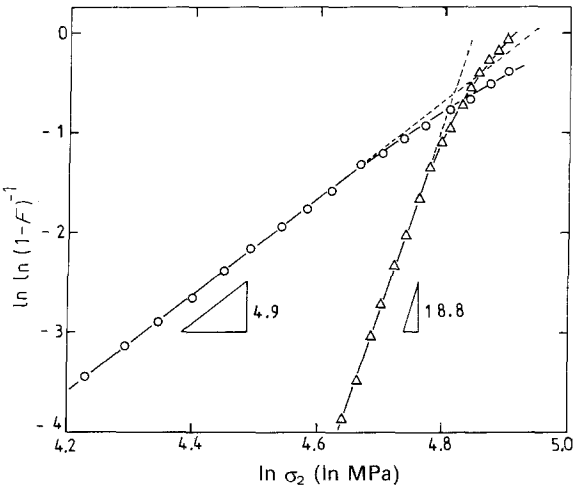

Figure 17 The probability of failure, $\ln\ln(1-F)^{-1}$, plotted against $\ln(\sigma_2)$ for the $0_2/90_6/0_2$ laminate with $w = 5$ ($\sigma_0 = 136$ MPa) and $w = 20$ ($\sigma_0 = 128$ MPa) based on the P method [7, 12] for an average of 30 specimens (runs).

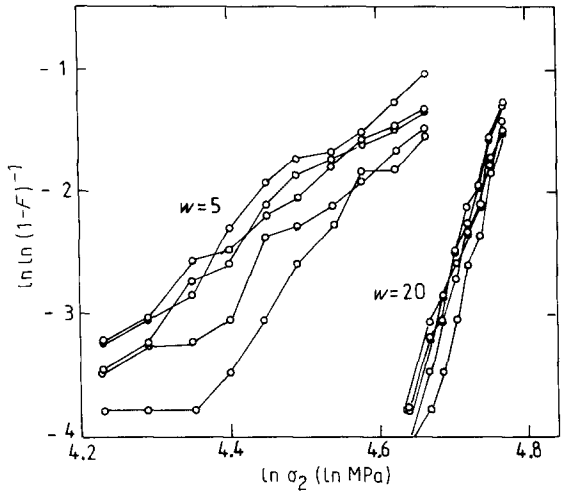

Figure 18 The probability of failure, $\ln\ln(1-F)^{-1}$, plotted against $\ln(\sigma_2)$ for five $0_2/90_6/0_2$ specimens (runs) for the cases of $w = 5$ ($\sigma_0 = 136$ MPa) and $w = 20$ ($\sigma_0 = 128$ MPa).

TABLE III The mean values of the Weibull parameters w and σ_0 calculated from the generated data (in Fig. 17) for 30 specimens (runs) by the P method [7, 12] compared with the original input parameters of the simulation experiment for the $0_2/90_6/0_2$ laminate

w		w	σ_0 (MPa)
5	Input	4.90	138
	Calculated	5.00	136
20	Input	18.8	128
	Calculated	20.0	128

TABLE IV The values of the Weibull parameters w and σ_0 for five specimens indicated in Fig. 18 calculated by the P method [7, 12] compared with the original input parameters of the simulation experiment for the $0_2/90_6/0_2$ laminate

w		w	σ_0 (MPa)
5	Calculated for	4.47	141
	each specimen	4.90	145
		4.97	138
		6.08	139
		5.16	139
	Average	5.14	136
	Original input	5.00	136
20	Calculated for	19.0	127
	each specimen	15.6	131
		16.4	130
		18.6	127
		20.6	129
	Average	18.0	129
	Original input	20.0	128

that the P method is also a good method if the number of test specimens is large.

Again, the applicability of this method to a small number of tests is examined. Fig. 18 shows examples of the plot of $\ln\ln(1-F)^{-1}$ against $\ln(\sigma_2)$ for five specimens. Although linearity is not very good, the values of w and σ_0 are determined by the least squares method, as shown in Table IV. There is some scatter, but the determined values are in good agreement with the original input values, suggesting that the P method is also applicable even for a small number of tests.

The P method has the advantage that the distribution of length of segments is not needed to determine the parameters and only the data on number of cracks (or average length) as a function of applied stress make it possible to determine the Weibull parameters.

The P method has been applied to the experimental results published previously [7, 12]. The determined values are $w = 10.47$ and $\sigma_0 = 158$ MPa for the $0_2/90_4/0_2$ laminate, $w = 7.55$ and $\sigma_0 = 145$ MPa for the $0_2/90_6/0_2$ laminate, and $w = 6.41$ and $\sigma_0 = 131$ MPa for the $0_2/90_{12}/0_2$ laminate. The residual strains, e_{r2}, have been measured as 0.448%, 0.433% and 0.394% for the $0_2/90_4/0_2$, $0_2/90_6/0_2$ and $0_2/90_{12}/0_2$ laminates, respectively [7]. These values are the input parameters in the simulation procedure and it is examined whether the multiple fracture data can be reproduced by the simulation procedure. Fig. 19 shows the results with the hatched regions for the experimental data [7] for four specimens. The

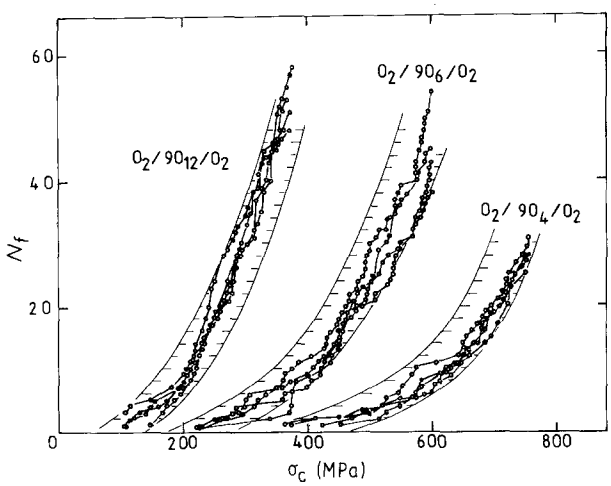

Figure 19 The relation between the number of cracks, N_f, and the applied stress, σ_c, for the different cross-ply laminates as a result of the present computer simulation in comparison with the original data [7] shown by the hatched regions. The Weibull parameters w and σ_0 in the computer simulation experiment were taken from [7]. $L_0 = 115$ mm.

experimental results are well reproduced, indicating again that the P method is useful to estimate the Weibull parameters.

4.5. The influence of the interlaminar shear strength on multiple fracture of the transverse ply

As shown in Section 4.1, the stress-carrying capacity of segments decreases quickly once interfacial debonding takes place. This means that the segments cannot be broken further once debonding occurs. Fig. 20 shows some examples of the results of the computer simulation representing the influence of interlaminar shear strength. It is obvious that fracture of the 90°-ply shows saturation at high applied stresses when the shear strength, τ_i, is low or when the number of transverse plies is large [12]. Another feature is that the lower the shear strength τ_i, the smaller becomes the number of cracks and the lower becomes the stress for saturation of transverse cracking.

The reduction in multiple fracture rate at high applied stress has been reported by Manders *et al.* [5] for a glass/epoxy laminate and by Garrett and Bailey [11] for a glass/polyester laminate. These results can be attributed to the plastic shear deformation of the matrix or interlaminar failure in the shear zone, which reduces the efficiency of stress transfer to the 90°-ply [12]. The present simulation demonstrates that the weak interface reduces the fracture rate at high applied stress, leading to a saturation of cracking.

4.6. Reduction in stress-carrying capacity due to multiple fracture

The stress–strain relations and the reduction in stiffness due to multiple fracture in the transverse ply have been studied by many researchers [9, 20, 21]. It has been demonstrated that multiple fracture leads to a reduction in stress-carrying capacity and in stiffness. In this section it is shown, how the stress-carrying capacity is reduced.

The stress-carrying capacity is expressed by the ratio $\sigma_c/\sigma_{c,0}$, in which σ_c is the stress in the composite in the damaged state (with transverse cracks) and $\sigma_{c,0}$ is the stress in the undamaged state at a certain strain. Fig. 21a shows some examples of the reduction in stress. The reduction in stress-carrying capacity increases with increasing applied stress, with the number of transverse cracks and with decreasing interlaminar shear strength. For a large interlaminar shear strength and a large scatter of the transverse strength ($w = 5$, case 1), multiple fracture starts at low applied stress but it progresses gradually due to the difference in the strength of the elements. Thus the reduction in stress-carrying capacity starts at relatively low applied stress and the reduction rate increases gradually. On the other hand, when the scatter is small ($w = 20$, case 3),

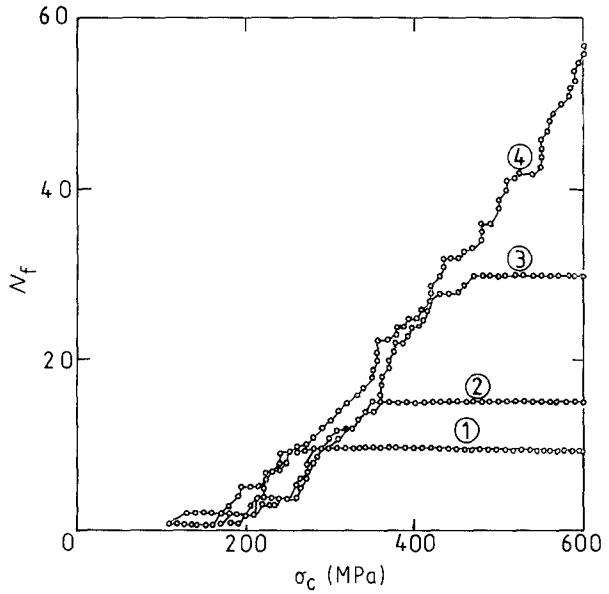

Figure 20 Influence of the interfacial bond strength on the number of cracks of the 90° ply, N_f, for the $0_2/90_6/0_2$ laminate with $w = 5$ ($\sigma_0 = 136$ MPa). $L_0 = 100$ mm; $\tau_i =$ (1) 250, (2) 300), (3) 350, (4) 500 MPa.

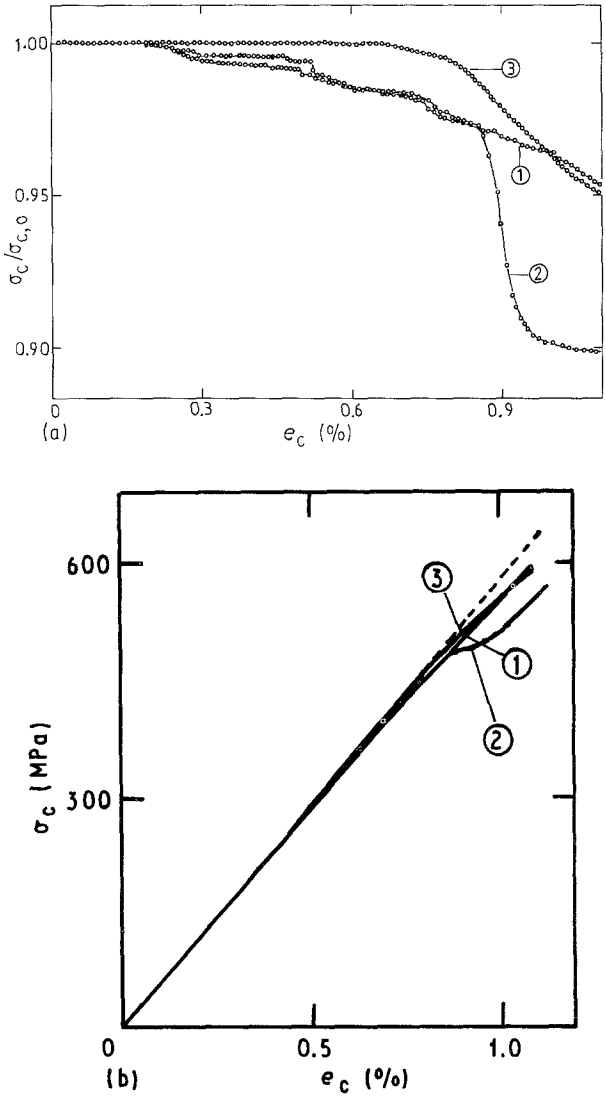

Figure 21 (a) The reduction in stress-carrying capacity due to multiple fracture of the 90°-ply in the $0_2/90_6/0_2$ laminate with (1, 2) $w = 5$ and (3) $w = 20$ ($\sigma_0 = 136$ MPa). $\tau_i =$ (1) 500, (2) 350, (3) 500 MPa. (b) Reduction in stress-carrying capacity, as shown by the stress-strain curve.

multiple fracture does not occur up to a relatively high applied stress but it progresses quickly once it starts. Now the reduction in stress-carrying capacity does only occur at a relatively high stress level but once it occurs, it increases quickly with increasing applied stress.

For a weak interlaminar shear strength, once interfacial debonding occurs, the reduction becomes very large. In this case, the reduction is clearly observed in the stress–strain curve shown in Fig. 21 (case 2) indicating that the contribution of the stress carried by the 90°-ply is very low. In the case where the stress-carrying capacity of the 90°-ply is almost completely lost due to debonding, the applied stress is carried only by the 0°-ply on the whole specimen length. Therefore, the Young's modulus of the specimen as a whole is given by $E_1 V_1$. In the present example for the $0_2/90_6/0_2$ laminate, the stress-carrying capacity is $E_1 V_1/(E_1 V_1 + E_2 V_2)$ where V_2, the volume fraction of 90°-ply, is 60%.

5. Conclusions

Multiple fracture of the transverse ply in cross-plied graphite–epoxy laminates was studied by means of a Monte Carlo simulation. The present work demonstrated that the smaller the scatter of strength of the 90°-ply, the higher becomes the threshold stress for multiple fracture to occur, and the more rapidly the length of segments decreases with increasing applied stress once multiple fracture takes place. Further, it was shown that if the interlaminar shear strength between 0° and 90°-plies is low, a saturation of transverse cracking occurs and that the reduction in effective stiffness or the reduction in stress-carrying capacity of the laminate increases with increasing applied stress or with number of cracks, especially when the interlaminar shear strength is low. Furthermore, it was proved that the methods to determine scale and shape parameters of the Weibull distribution for the strength of the 90°-ply, as proposed by Manders *et al.* and Peters, are useful even for a small number of test specimens.

Acknowledgement

One of the authors (S.O.) thanks Professor Dr W. Bunk, DLR, Cologne, for the invitation to his Institute and his encouragement.

References

1. A. KELLY and W. R. TYSON, *J. Mech. Phys. Solids* **13** (1965) 329.
2. A. PARVIZI, K. W. GARRET and J. E. BAILEY, *J. Mater. Sci.* **13** (1978) 195.
3. D. L. FLAGGS and M. H. KURAL, *J. Comp. Mater.* **16** (1982) 103.
4. F. W. CROSSMAN, A. S. D. WANG, ASTM STP 775 (American Society for Testing and Materials, Philadelphia, PA, 1982) p. 118.
5. P. W. MANDERS, T. W. CHOU, J. R. JONES and J. W. ROCK, *J. Mater. Sci.* **18** (1983) 2876.
6. H. FUKUNAGA, T. W. CHOU, P. W. M. PETERS and K. SCHULTE, *J. Compos. Mater.* **18** (1984) 339.
7. P. W. M. PETERS, *ibid.* **18** (1984) 545.
8. A. PARVIZI and J. E. BAILEY, *J. Mater. Sci.* **13** (1978) 2131.
9. A. L. HIGHSMITH, W. W. STINCHCOMB and K. L. REIFSNIDER, VPI-E-81.33, Virginia Polytechnic Institute and State University, Blacksburg, VA, USA, November 1981.
10. K. L. REIFSNIDER, E. G. HENNEKE and W. W. STINCHCOMB, "Defect-property Relationships in Composite Materials", ASML-TR-76-81, Part IV (June, 1979).
11. K. W. GARRETT and J. E. BAILEY, *J. Mater. Sci.* **12** (1977) 157.
12. P. W. M. PETERS and T. W. CHOU, *Composites* **18** (1987) 40.
13. A. S. D. WANG and F. W. CROSSMAN, *J. Compos. Mater. Suppl.* (1980) 71.
14. A. S. D. WANG, "Advances in Composite Materials", Vol. 1 (Pergamon, Oxford, 1980) p. 170.
15. S. OCHIAI and Y. MURAKAMI, *Trans. Jpn Inst. Metals* **18** (1977) 384.
16. S. OCHIAI and K. OSAMURA, *Z. Metallkde* **77** (1986) 255.
17. *Idem, J. Mater. Sci.* **21** (1986) 2735.
18. S. OCHIAI, T. UEHARA and K. OSAMURA, *ibid.* **21** (1986) 1020.
19. W. WEIBULL, *J. Appl. Mech.* **28** (1951) 293.
20. J. M. WHITNEY, C. E. BROWNING and G. C. GRIMES, "Composite Materials in Engineering Design" (ASM, 1972) p. 441.
21. H. T. HAHN and S. W. TSAI, *J. Compos. Mater.* **8** (1974) 288.

Received 27 November 1989
and accepted 18 July 1990